SOLAR ASSISTED REACTORS FOR METHANE PYROLYSIS IN LIQUID METAL MEDIUM

Elisa Alonso*, Luis Francisco González-Portillo, Alberto Abánades

Universidad Politécnica de Madrid ETSII-UPM, Department of Energy Engineering, Madrid, Spain

*Corresponding Author: elisa.alonso@upm.es

ABSTRACT

Methane pyrolysis is as an alternative method for hydrogen production, which offers the additional advantage of generating high-value solid carbon as a co-product. To address challenges such as carbon deposition in conventional gas-phase reactors, the use of liquid metal mediums such as tin is proposed. Thinking in feeding the process with clean and renewable energy, this paper investigates two conceptual approaches for integrating concentrated solar energy into the methane pyrolysis process using liquid tin as the medium. The first approach involves directly irradiating the pyrolysis column, while the second utilizes an external receiver to heat the tin before transferring it to the column. Basic thermal modeling and analysis are conducted for both approaches to evaluate their feasibility and compare them. Results indicate that while the direct irradiation approach offers simplicity in design, the receiver-based approach provides better utilization of solar radiation and less thermal losses.

1 INTRODUCTION

Ecological transition, including transition to a sustainable energetic model, is mandatory in order to revert climate change and the current unsustainable social and economic model. In this context, the European Union delivered the European Green Deal aiming to make Europe climate-neutral by developing cleaner sources of energy and green technologies.

The biggest challenge of the energy sector is the complete substitution of fossil fuels by renewable and clean energy sources. Hydrogen is seen as potential contributor towards a sustainable future, serving not only as an alternative and non-polluting fuel for air, sea and land transportation as well as industry and buildings, but also as an energy carrier that enhances the dispatchability of renewable energy. Importantly, there are also several industry sectors for which hydrogen is a crucial feedstock.

Inconsistently, 96% of hydrogen is currently produced from fossil fuels using thermal methods that result in CO_2/CO emissions. The main methods are steam reforming of natural gas, partial oxidation of hydrocarbons and coal gasification. The remaining 4 % comes from water electrolysis which is still very expensive (around 5 €/kg H_2), and its massive deployment might stress water and critical raw material resources. In addition, electrolysis is facing the challenge to reach the clean production scale of large capacity industries in the hard-to-decarbonize sectors

Methane pyrolysis, also known as methane cracking, a cheap and CO_2 free alternative hydrogen production process. It also produces high-value carbon (carbon black or graphite) as a co-product, and it has been a subject of research interest for decades (Da Costa Labanca, 2020). The process consists in thermally dissociating the methane molecules (CH_4) into hydrogen (H_2) and high purity solid carbon (C) according to:

$$CH_4 \rightarrow C + 2H_2 \qquad \Delta H\ (298K) = 74.9\ kJ/mol$$

The reaction co-product, carbon, is currently one of the top 50 global commodities, with a market valued at 20.6 billion € in 2023 and is a critical raw material likely to become more stressed by the demand of

https://doi.org/10.52202/077185-0070

traditional industries, as steel manufacturing, and the emerging of new technologies as graphene, or Li-ion batteries. The demand of carbon materials, in particular graphite, will be multiplied by a factor 14 according to a European Commission foresight study on critical materials, from 250 kt/year to 3.5 Mt/year in 2050.

Pyrolysis avoids the generation of CO_2 or CO emissions as the carbon atoms present in methane are transformed into solid carbon. Apart from its low cost, this is the main advantage of this method over other thermal processes starting from fossil fuels. Moreover, the process becomes entirely clean and sustainable when both the methane feedstock and the thermal energy originate from clean and renewable sources (Postels et al., 2016).

2 METHANE PYROLYSIS IN LIQUID MEDIA

A common issue in typical gas-phase methane pyrolysis reactors is carbon deposition on walls and ducts, leading to undesired blockages. This drawback can be solved by using liquid metal reaction media. Its main advantage is a simplified management of the carbon particles into the reactor via flotation: carbon particles naturally rise to the top of the reactor owing to the difference in density with the liquid bath. Carbon can then be mechanically recovered from the reactor top and exploited as a high-value co-product, thereby depositions and blockages are avoided. Performing the reaction in liquid metal effectively removes oxygen from the process without the need to use any sweeping gas (Abánades et al., 2011). Moreover, the liquid metal bath facilitates the thermal management of the device, thanks to the high thermal diffusivity of the reaction medium which leads to improved temperature homogeneity, fundamental for process scalability (Geißler et al., 2015). Thermal energy present in liquid metal is taken by the endothermic reaction to bring forth the methane dissociation. A conceptual approach to the liquid metal reactor for methane pyrolysis is represented in Figure 1.

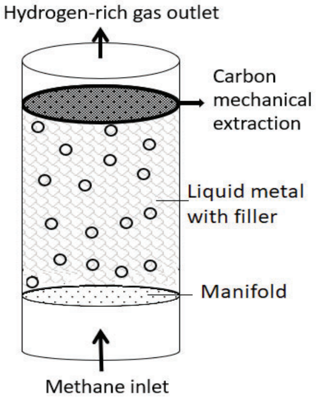

Figure 1. Concept of gas pyrolysis reactor in liquid metal reactor

The reactor consists of a column of significant height filled with a molten metal, for example, tin, which is being considered in this work. It must operate at a high enough temperature (above 800-1000 ºC approximately) to originate the spontaneous methane pyrolysis. Gas is injected through a manifold with a set of orifices located in the lower section, allowing for the formation of gas bubbles. These bubbles ascend through the column while increasing their temperature and are transformed into hydrogen and carbon. To extend the gas path through the metal bath and increase residence time for CH_4 splitting, an inert packed bed can be immersed in the liquid metal. While generated hydrogen flows outside through a duct at the column top, carbon particles are accumulated on top of liquid tin due to the density difference, and can be subsequently mechanically removed.

Although different sources of energy can supply the heat required to melt and keep the liquid metal melted at high temperature, this technology will only become truly meaningful from the sustainability

https://doi.org/10.52202/077185-0070

point of view if the energy origin is clean and renewable. This study specifically focuses on Concentrating Solar Energy (CSE), a technology with well-known features and advantages as a heat source. The objective is to explore and analyze alternatives for integrating concentrated solar flux into liquid metal reactors. This is a preliminary stage in the development of an optimized solar liquid-metal reactor for methane pyrolysis.

3 STRATEGIES FOR SOLAR HEATING

Solar reactors are particular cases of solar receivers where the absorbed heat is employed to carry out endothermic chemical reactions. Typically, solar reactors are classified based on how the solar flux reaches the reactants (Alonso and Romero, 2015). Thus, in directly irradiated reactors the primary absorber is a reactant that undergoes a chemical transformation as a result of an increase in its thermal energy. In indirect irradiated reactors an intermediary medium, frequently opaque walls, absorbs the solar radiation and heats up the reactants by conduction, convection and/or radiation emission.

From the perspective of the mentioned categories, a solar liquid-metal reactor should be strictly considered an indirect reactor. The heat transfer from solar radiation occurs towards the metal, which then releases it to the gaseous reactant. In fact, the feasibility of directly irradiating the liquid metal to elevate its temperature is likely to be limited by its optical properties. Although decreasing with temperature and wavelength, typical solar hemispherical reflectivity of metals, including tin, is high. (Siegel, 1975, Spisz et al., 2020)

Two different approaches are presented here for coupling solar radiation to the reactor with the aim of melting and maintaining the molten tin at a high temperature. The first approach is based on irradiating the external wall of the column containing the tin, where the gas is bubbled to perform its pyrolysis.

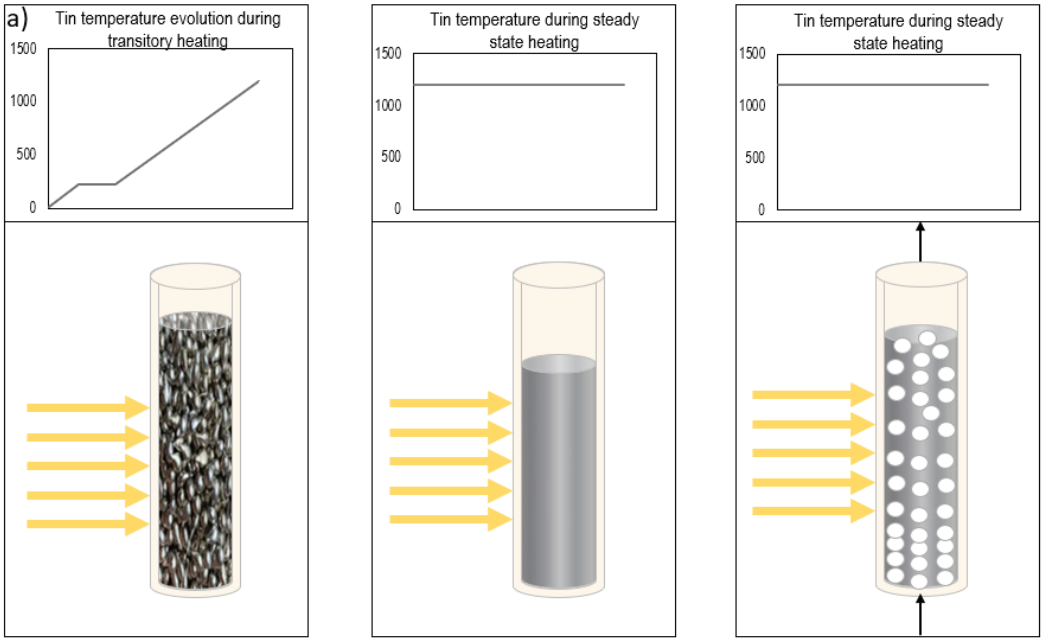

High flux of radiation reaches the column containing tin at ambient temperature. Its temperature in its solid state rises due to the change in sensible energy, Then, the tin undergoes melting and continues to overheat until it reaches the set point temperature.

Only the radiation flux required to offset losses maintaining constant tin temperature is supplied at this stage.

When CH_4 begins bubbling into the column, an energy sink appears in the tin. This should be compensated for by an additional radiation flux

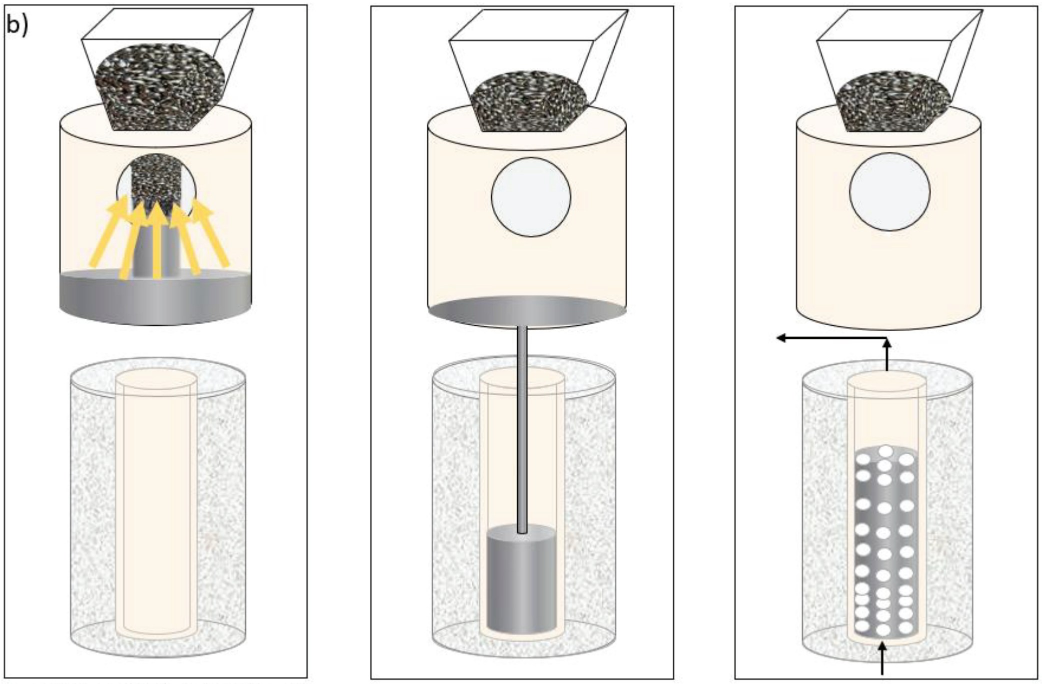

A solar receiver optimized to absorb radiation is employed to melt and heat up the tin until the set temperature is reached. The receiver can be a cavity type or another design. Temperature evolution is equivalent to a).

Liquid tin at high temperature is transfered to the insulated column.

Once the tin is in the column CH_4 begins bubbling and continues until the tin temperature falls below a set threshold.

Figure 3. Two approaches for integrating concentrating solar flux in a liquid metal CH_4 pyrolysis process. Case a): Direct heating of the liquid metal column through its external wall. Case b): Heating the tin in a solar receiver and transferring in liquid state and high temperature to the column.

The radiation flux reaches the column, and heat is transferred to the metal through conduction.

The second approach involves an external receiver with tin serving as the heat transfer fluid (HTF), which heats up and flows at high temperature into the column. The column should be adequately thermally insulated so that the tin temperature primarily decreases due to the enthalpy consumed by the methane dissociation reaction. Once the tin temperature falls below a set threshold, it would be extracted, and the column subsequently refilled.

Basic analytical models are presented next for both strategies and are illustrated in Figure 3. The aim of the models is not to obtain a precise characterization of the mentioned thermal systems but to understand the features of each conceptual approach and establish a comparison between them.

4 THERMAL MODELING

Preliminary thermal modeling for cases a) and b) are presented in this section, under the assumptions and simplifications outlined below:

- The evaluation is made for a laboratory-scale reactor which will be irradiated by a concentrator prototype yet to be defined. The mass of tin (m_{tin}) in the pyrolysis column is fixed at 100 kg.

- The column is made of a conductive silicon carbide, with an assigned absorptivity, α, of 0.85 (Gallo et al., 2019) and the thermal properties listed in Table 1 for the whole range of temperature.
- Column dimensions are 0.18 m in inner diameter (D_i), 0.2 m in outer diameter (D_o) and 1 m in high.
- The temperature of the column inner wall, $T_{w,i}$ is considered to be the same as the tin temperature (T_{Sn}).
- In transient heating, both SiC of the column and tin are assumed to increase their temperature simultaneously, acknowledging that this simplification does not precisely reproduce reality. The assumption is made for practical purposes to facilitate the estimation of the required heating time.
- Solar receiver in case b) is assumed to be a cavity with an assigned absorptivity of 0.95.
- The temperature set at the tin after been heated up is 1200 ºC. For case b), tin cools down once it is transferred to the column. The threshold temperature indicating the need of emptying the column of tin and refill it with hotter liquid metal is set in 900 ºC.
- Thermal losses during the liquid tin transfer from the receiver to the column are neglected.
- The spot generated by the solar concentrator on the column is a circle of 0.2 m in diameter (D_{spot}) with a Gaussian incident flux distribution, assuming a constant peak concentration ratio of 7200 suns (I_{max}=7200 kW/m^2) and standard deviation, σ, of 0.06 m. Figure 4 shows the integration of which in a circle with a diameter of 0.2 m results in a power of 100 kW (q_{sun}).

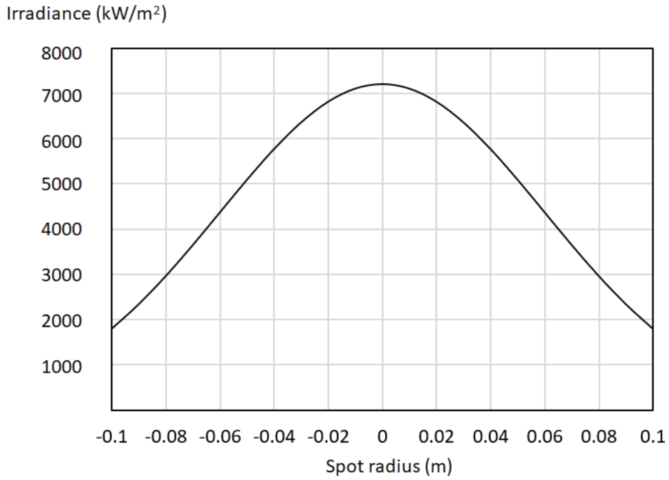

Figure 4. Solar irradiance distribution considered on the column external wall, with radius = *r*.

Equation 1 is employed to calculated the power, *P*, corresponding to a certain diameter solar spot with gaussian distributed irradiance.

$$P = 2\int_0^{0.1} I_{max} \cdot e^{-\frac{r^2}{2\sigma^2}}\, 2\pi r dr \tag{1}$$

4.1 Case a). Irradiated column.

Thermal power absorbed by the column is the product of the received power, q_{sun}, by the absorbance, α, as expressed by Equation 2.

$$q_{abs} = \alpha \cdot q_{sun} \tag{2}$$

To model case a), the process is divided into three stages of duration t_1, t_2 and t_3.

Initially, the tin undergoes an increase in sensible heat until it reaches the melting temperature. The time invested in this heating stage, denoted as t_1, is determined by Equation 3. This equation also accounts for the simultaneous increase in sensible heat for the SiC column. Thermal losses by convection and

https://doi.org/10.52202/077185-0070

radiation can be negligible for this stage and the next one if compared to q_{abs}. For example, when the external wall of the column is close to the melting temperature of tin ($T_{melt,Sn}$), radiative emission accounts for only a small fraction (1%) of the absorbed power, and convective losses are even lower.

$$t_1 = \frac{m_{tin} \cdot \int_{T_{amb}}^{T_{melt}} Cp_{tin,solid} \cdot dT + m_{SiC} \cdot \int_{T_{amb}}^{T_{melt}} Cp_{SiC} \cdot dT}{q_{abs}} \tag{3}$$

where *Cp* represents the specific heat of tin and SiC.

Subsequently, the melting of Sn will occur, and its duration, denoted as t_2, can be estimated based on its latent heat, as given in Equation 4.

$$t_2 = \frac{m_{tin} \cdot H_{melt}}{q_{abs}} \tag{4}$$

For the estimation of t_1 and t_2 following Equation 3 and 4, q_{sun} is considered as the maximum value provided by the solar concentration system, which is 100 kW. This implies a very high heating rate. In practice, such rapid heating may not be feasible, as materials are likely to experience thermal shocks even with high thermal conductivity. Therefore, the time required to heat the system until the tin melts is estimated using various fractions of the maximum thermal power provided by the concentrator.

Table 1 compiles the properties of tin utilized for this model.

Table 1: Sn and SiC properties utilized for the present model.

Tin	**Thermal conductivity, *k* (W/m·K) (600-1200 ºC)**	0.0234T+16.171
	Thermal conductivity, *k* (W/m·K) (0-100 ºC)	66.8
	Melting temperature, T_{melt} (ºC)	231.9
	Latent heat of melting, H_{melt} (kJ/kg)	59
	Specific heat, *Cp* (J/kg·K) (600-1000 ºC)	-0.0003T^2+0.5119T+17.975
	Specific heat, *Cp* (J/kg·K) (0-100 ºC)	227
Silicon carbide	**Thermal conductivity, *k* (W/m·K)**	120
	Density (kg/m^3)	3100
	Specific heat, Cp (J/kg·K)	750

In next step, liquid tin will undergo a further increase in sensible energy until reaching the maximum temperature. For this estimation, the maximum temperature is fixed at 1200 ºC. The time dedicated to the second phase of sensible heat gain is referred to as t_3 and expressed by Equation 5. Now, the model incorporates a factor, F_{loss}, ranging from 0 to 1 to consider radiative thermal losses from the external wall of the column. Neglecting these losses at elevated operating temperatures could introduce a significant source of error. The factor is estimated as the average of the emissive power over the temperature range from T_{melt} to T_{max}, despite the external wall temperature not exactly matching the tin temperature. It is detailed in Equation 6.

$$t_3 = \frac{m_{tin} \cdot \int_{T_{melt}}^{T_{max}} Cp_{tin,liquid} \cdot dT + m_{SiC} \cdot \int_{T_{amb}}^{T_{melt}} Cp_{SiC} \cdot dT}{q_{abs} \cdot F_{loss}} \tag{5}$$

$$F_{loss} = \frac{q_{abs} - \left(\frac{\int_{T_{melt}}^{T_{max}} \varepsilon_{SiC} \sigma \pi D_O L (T^4 - T_{sur}^4) dT}{T_{max} - T_{melt}} \right)}{q_{abs}} \tag{6}$$

Thermal transfers in steady-state are analyzed according to the following diagram.

https://doi.org/10.52202/077185-0070

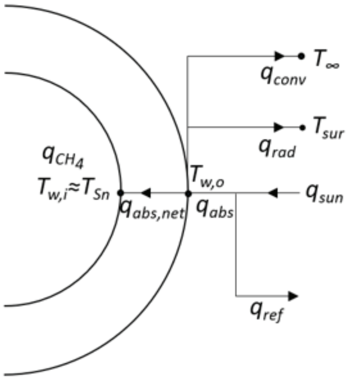

Figure 5. Diagram representing heat transfers for the tin column.

The net heat absorbed by the tin, $q_{abs,net}$, is the result of the heat balance on the external wall of the column and is expressed by Equation 7. This thermal power is transferred to the tin by conduction, however its modelling is not trivial because the radiation flux is concentrated on a specific zone of the column and it is conducted in radial and longitudinal directions. Therefore, such calculation is beyond the scope of this basic model. To estimate convective (Equation 8) and radiative (Equation 9) losses, half of the column external surface is considered, with the assumption that the other half is well insulated. Additionally, the exposed area is assumed to be at the maximum temperature of the tin, that is 1200 ºC, which will be close to the real temperature due to the high conductivity of SiC.

$$q_{abs,net} = \alpha q_{sun} - q_{conv} - q_{rad} \tag{7}$$

$$q_{conv} = h \cdot D_o \cdot 0.5 \cdot \pi \cdot L \cdot (T_{w,o} - T_\infty) \tag{8}$$

$$q_{rad} = \varepsilon_{SiC} \cdot \sigma \cdot D_o \cdot 0.5 \cdot \pi \cdot L \cdot (T_{w,o}^4 - T_{sur}^4) \tag{9}$$

where $T_{w,o}$ is the temperature of the column external wall, T_∞ is the ambient temperature and T_{sur} is the surroundings temperature to which the column emits radiation. L is the column height and D_o the external diameter. The convective coefficient, h, is calculated using the Nusselt number for natural convection around a vertical tube, which does not satisfy the condition $D/L \geq 35/Gr^{0.25}$. For this case, the Churchill–Chu correlation (Churchill and Chu, 1975)for a vertical plate (Equation 10) can be used to calculate the Nusselt number for a vertical plate (Nu_{vp}). Then, the Nusselt number for a vertical narrow cylinder, Nu_{vc}, and h coefficient, are obtained as indicated by Equations 11 and 12.

$$Nu_{vp} = 0.68 + 0.67 Ra_L^{1/4} \left[1 + \left(\frac{0.492}{Pr}\right)^{9/16}\right]^{-4/9} \tag{10}$$

where Ra_L is the Rayleigh number for calmed air at ambient temperature surrounding a tube of 1 m in height at 1200 ºC, having a value of $3.14 \cdot 10^5$ and Pr is the Prandtl number of air at ambient temperature and has a value of 0.68.

$$Nu_{vc} = Nu_{vp} \cdot \frac{\frac{1.8}{Nu_{vp}} \cdot \frac{L}{D_O}}{ln\left(1 - \frac{1.8}{Nu_{vp}} \cdot \frac{L}{D_O}\right)} \tag{11}$$

$$h = \frac{Nu \cdot L}{k_{air}} \tag{12}$$

where k_{air} is the thermal conductivity of air at ambient temperature and has a value of 0.04 W/m·K.

When CH_4 is introduced in the column with the tin at 1200 ºC the endothermic splitting begins. The power consumed by the methane splitting into H_2 and C is denoted as q_{CH4} and corresponds to the mass flow rate of bubbled CH_4 multiplied by its splitting reaction enthalpy, ΔH_r, which is 4666.45 kJ/kg (Abánades et al., 2013). Applying a heat balance to the inner volume of the column, the $q_{abs,net}$ will be equal to the power consumed by the reaction, as expressed in Equation 13. This allows for the calculation of the methane mass flow rate that can be pyrolyzed, given the net thermal power absorbed by the tin under specific conditions

$$q_{abs,net} = q_{reac} = \Delta H_r \cdot \dot{m}_{CH4} \tag{13}$$

4.2 Case b). Irradiated receiver.

In case b) solar radiation impinges on the receiver. For this model, it is a cavity receiver with an absorptance of 0.95, therefore q_{abs} is calculated according to Equation 2. The tin, previously charged into a hopper, falls and accumulates into the cavity while being heated up by the solar radiation. The working mode is not continuous but in batches of 100 kg, which are then transferred to a column of the same dimensions as in case a). Equations 3, 4, 5, and 6 are also applied here to estimate the time required for the tin to reach 1200 ºC in a liquid state. The difference is that this time, the tin heating up takes place in the cavity, so the thermal capacity of the column is not accounted for.

Thermal transfers for the cavity receiver in steady-state are depicted in the diagram shown in Figure 6. While solving this thermal balance is not essential for this procedure, it is calculated here to explore the possibility of retaining the liquid tin in the cavity for a certain duration, if necessary. Convective losses are neglected under the assumption of no wind around the receiver. The heat balance to the cavity is expressed by Equation 14.

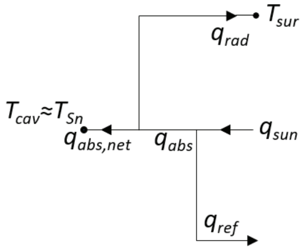

Figure 6. Diagram representing the heat transfers for the cavity receiver.

$$q_{abs,net} = q_{abs} - \varepsilon_{cav} \cdot \sigma \cdot A_{cav}(T_{cav}^4 - T_{sur}^4) \tag{14}$$

Where ε_{cav} and A_{cav} are the emissivity and aperture area of the cavity. When liquid tin is transferred from the cavity to the column, CH_4 can be injected to initiate the chemical reaction. The tin temperature begins to decrease due to conduction losses toward the insulation and, mainly, the enthalpy consumed by the reaction. Since the second contribution is much higher than the first one, conductive losses are neglected in this model. A threshold temperature of 900 ºC is stablished so that once the tin is cooled down to 900 ºC, it is extracted from the column and the column is refilled with hotter tin from the cavity. The tin solidifies outside the column, forming drops that are then mechanically transferred to the hopper to be reheated. The heat released by the tin during its cooling and solidification can be recovered and reutilized for various applications. It represents a valuable source of waste. t_4 is the time until the tin cools to 900 °C.

$$t_4 = \frac{m_{tin} \cdot \int_{1200}^{1000} Cp_{tin,liquid} \cdot dT}{\dot{m}_{CH4} \cdot \Delta \mathrm{H}_r} \tag{15}$$

5 RESULTS

5.1 Case a). Irradiated column.

From the transient model, estimated times to reach melting and maximum temperature are provided (Equations 3 to 6). In Table 2, t_1, t_2 and t_3 are given for a supplied solar power of 100 kW.

Table 2. Duration of sensible (in solid and liquid states) and latent heat gains for 100 kW of solar input in case a).

	Type of energy gain	Time (s)
t_1	Sensible heat in solid state	89
t_2	Latent heat	69
t_3	Sensible heat in liquid state	527

If the solar power is reduced, either intentionally to avoid materials issues or due to weather conditions, heating times will extend. Figure 7 considers scenarios of different values of q_{sun}. The lower of the considered powers will not be sufficient to achieve 1200 ºC due to the increasing radiative losses with temperature, implying the need for a higher fed power.

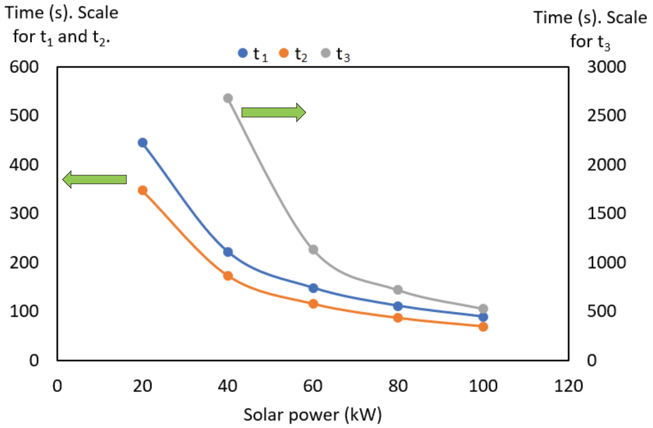

Figure 7. Estimated heating times for sensible and latent energy gain versus supplied solar power in case a).

Equations 7 to 13 have been solved and both the inputs and outputs are summarized in Table 3.

Table 3. Inputs and outputs of the steady-state model for case a).

Inputs			Outputs		
Parameter	**Units**	**Value**	**Parameter**	**Units**	**Value**
q_{sun}	W	100000	q_{ref}	W	15000
α	--	0.85	q_{abs}	W	85000
D_o	m	0.2	$q_{abs,net}$	W	13535
$T_{w,o}$	ºC	1200	q_{conv}	W	273
h	$W/m^2 \cdot K$	0.74	q_{rad}	W	71192
L	m	1	$\dot{m}_{CH4}$	kg/s	0.003
T_∞	ºC	25			
σ	$W/m^2 \cdot K^4$	$5.67 \cdot 10^{-8}$			
T_{sur}	ºC	23			
ΔH_r	J/kg	4666450			

https://doi.org/10.52202/077185-0070

Therefore, for a net absorbed power of 13535 W, 0.003 kg/s or 10.4 kg/h of CH_4 could be pyrolyzed if only energy aspects were considered.

5.2 Case b). Irradiated receiver.

Equations 3, 4, 5, and 6 were solved for this case to determine the heating times presented in Table 4. In equations 4 and 5, m_{SiC} is zero because this parameter corresponds to the column mass, which is not applicable in this case.

Table 4. Duration of sensible (in solid and liquid states) and latent heat gains for 100 kW of solar input in case b)

	Type of energy gain	Time (s)
t_1	Sensible heat in solid state	80
t_2	Latent heat	62
t_3	Sensible heat in liquid state	361

As analyzed in case a), scenarios with reduced solar power are also considered in this case. Heating times will increase when solar power is decreased, as shown in Figure 8.

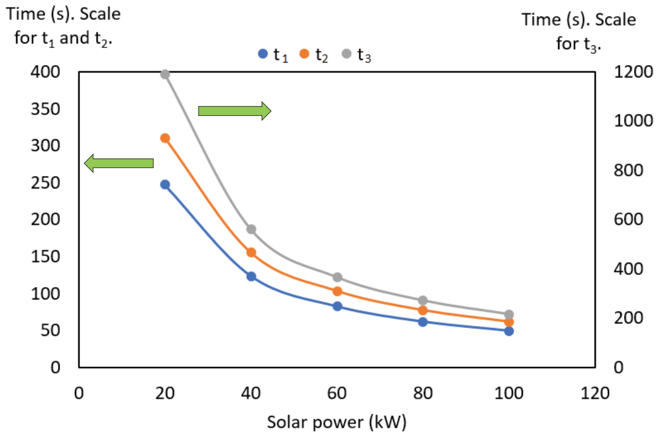

Figure 8. Estimated heating times for sensible and latent energy gain versus supplied solar power in case b).

Table 5 shows the input and output parameters from the steady-state model applied to the cavity receiver as represented in Figure 6. D_a is the diameter of the cavity aperture.

Table 5. Inputs and outputs of the steady-state model for case b).

Inputs			Outputs		
Parameter	Units	Value	Parameter	Units	Value
q_{sun}	W	100000	q_{ref}	W	5000
α	--	0.95	q_{abs}	W	95000
D_{spot}	m	0.2	$q_{abs,net}$	W	87608
D_a	m	0.2	q_{rad}	W	7117
T_{Sn}	ºC	1200	q_{ref}	W	5000
T_∞	ºC	25			
σ	$W/m^2 \cdot K^4$	$5.67 \cdot 10^{-8}$			
T_{sur}	ºC	23			

According to this conceptual design, when 100 kg of tin is at 1200 ºC, it is transferred from the cavity to the column, where the CH_4 is injected to initiate pyrolysis. Equation 15 is utilized to estimate the time it takes for the tin to decrease its temperature from 1200 to 900 ºC, considering the enthalpy consumed by methane splitting. For comparative purposes, the same mass flow rate calculated for case a) (0.003 kg/s) is used to estimate t_4, resulting in 493 s, which is very close to the total heating time (503 s). That means that while one batch of hot tin is being used in the column as reaction medium, another is being heated in the receiver, enabling the system to pseudo-continuously work during the availability of radiation.

6 SUMMARY AND CONCLUSIONS

Two conceptual approaches, named as case a) and case b), are proposed for coupling solar irradiation into the methane pyrolysis reactor within a liquid tin medium. Both approaches involve melting and heating the tin to approximately 1200 ºC, facilitating methane reduction without the need for a catalyst. In case a), the pyrolysis column is irradiated to heat up the tin inside it, while in case b), a solar receiver is incorporated to heat the tin inside it before being transferred to the column. Following, some characteristics linked to approaches a) and b) are highlighted and where applicable, compared.

- Case a) construction is much simpler than case b) in construction as it involves only one key component (the column) instead of two (the receiver and the column).

- For a given solar concentration system able to supply 100 kW of solar power, assuming maximum power and ideal conditions (no material issues, no significative thermal losses apart from those considered in the model), transient heating would last 685 s for case a) and 503 s for case b), that is 36% faster in case b).

- In case a) 20 kW is not enough solar power for the tin to reach 1200 ºC during transient heating. However, in case b), the maximum temperature would be achieved in about half an hour with a 20-kW solar concentrator. That means that a 20-kW concentrator would be valid option for case b) while case a) would always require a more powered solar system.

- A deeper analysis of the design and construction costs for both cases a) and b) should be carried out. While case b) involves two key components compared to just one in case a), the solar concentration system required for case a) is more technically demanding and, therefore, likely to incur higher expenses.

- The necessity of transferring hot tin from the cavity to the column is a drawback associated with case b). However, this operation mode allows for more flexibility in the operation, as the tin temperature can be controlled in the cavity and just transferred to the column when required or desired. Pyrolysis can be conducted within the well-insulated column for 493 seconds, maintaining the tin temperature above 900 ºC. While it is required to determine if reducing the tin temperature from 1200 to 900 ºC significantly impacts H_2 production, these results suggest that a quasi-continuous operation mode could be imposed for the system b).

- Tin extracted at 900 ºC has a large amount of thermal energy that can be recovered and reused for various applications.

- Regarding the current approaches, both cases seem to produce similar amount hydrogen as final product. However, thermal losses unavoidable for case a) can be recovered in case b).

In summary, the main advantage of case a) is the system simplicity which could have a direct repercussion in design and construction costs. However, as the column cannot be insulated thermal losses are high and a powerful solar concentration system is required to reach the maximum temperature. Conversely, in case b), the system is more complex, involving a receiver, a column, and a

https://doi.org/10.52202/077185-0070

tin transfer system between them. Despite this complexity, radiation is better utilized in the receiver, favoring the transient heating of case b), which is faster and more affordable with a smaller concentrator. Furthermore, the system offers greater flexibility, as the column can be well insulated to minimize heat loss, and heat can be recovered from the controlled cooling of the tin.

REFERENCES

Abánades, A., Rubbia, C., Salmieri, D., 2013. Thermal cracking of methane into Hydrogen for a CO_2-free utilization of natural gas. International Journal of Hydrogen Energy 38, 8491–8496.

Abánades, A., Ruiz, E., Ferruelo, E.M., Hernández, F., Cabanillas, A., Martínez-Val, J.M., Rubio, J.A., López, C., Gavela, R., Barrera, G., Rubbia, C., Salmieri, D., Rodilla, E., Gutiérrez, D., 2011. Experimental analysis of direct thermal methane cracking. Int J Hydrogen Energy 36, 12877–12886.

Alonso, E., Romero, M., 2015. Review of experimental investigation on directly irradiated particles solar reactors. Renewable and Sustainable Energy Reviews 41, 53–67.

Churchill, S., Chu, H., 1975. Correlating Equations for Laminar and Turbulent Free Convection from a Vertical Plate. International Journal of Heat and Mass Transfer 18, 1323–1329.

Da Costa Labanca, A., 2020. Carbon black and hydrogen production process analysis. 45, 25698–25707. Int. J. Hydrogen Energy. 45, 25698–25707.

Gallo, A., Alonso, E., Pérez-Rábago, C., Fuentealba, E., Roldán, M.I., 2019. A lab-scale rotary kiln for thermal treatment of particulate materials under high concentrated solar radiation: Experimental assessment and transient numerical modeling. Solar Energy 188, 1013–1030.

Geißler, T., Plevan, M., Abánades, A., Heinzel, A., Mehravaran, K., Rathnam, R.K., Rubbia, C., Salmieri, D., Stoppel, L., Stückrad, S., Weisenburger, A., Wenninger, H., Wetzel, T., 2015. Experimental investigation and thermo-chemical modeling of methane pyrolysis in a liquid metal bubble column reactor with a packed bed. Int J Hydrogen Energy 40, 14134–14146.

Postels, S., Abánades, A., von der Assen, N., Rathnam, R.K., Stückrad, S., Bardow, A., 2016. Life cycle assessment of hydrogen production by thermal cracking of methane based on liquid-metal technology. Int J Hydrogen Energy 41, 23204–23212.

Siegel, E., 1975. Optical reflectivity of liquid metals at their melting temperatures. Phys Chem Liquids 5, 9–27.

Spisz, E.W., Weigund, A.J., Bowmun, R.L., Juck, J.R., 2020. Solar absorptances and spectral reflectances of 12 metals for temperatures ranging from 300 to 500 K.

ACKNOWLEDGEMENT

This work has been carried out within the BrainEn Missions project with exp. MIG-20211033 in the framework of the Recovery, Transformation and Resilience funded by CDTI.

https://doi.org/10.52202/077185-0070